Cerro Casale Alteration Report

Alteration Mapping Using ASTER Satellite Imagery and Spectral Matching with Deep Learning Algorithms

Author:

Margaret McPherson (P.Geo.)

PhotoSat

Better Data for Better Decisions

Contact Information

Head Office

PhotoSat Information Ltd.
#580-1188 West Georgia Street
Vancouver BC V6A4E2
1-604-681-9770 | info@photosat.ca

Author

Margaret McPherson (P. Geo.)
Product Manager - Alteration
margaret.mcpherson@photosat.ca

Date of Publication
First: September 1st, 2019
Revised: September 26th, 2022

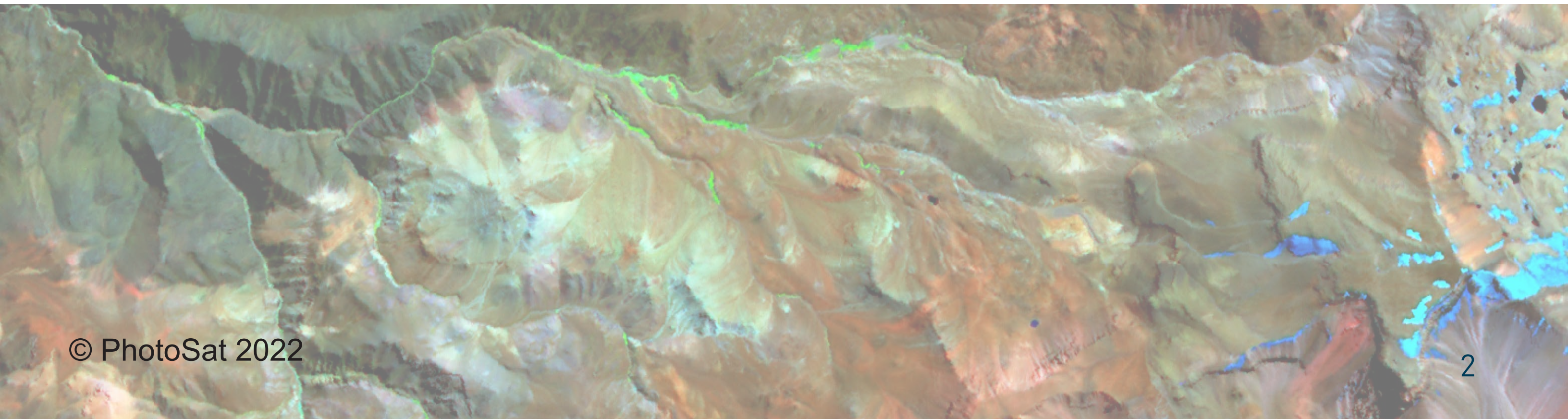

Contents

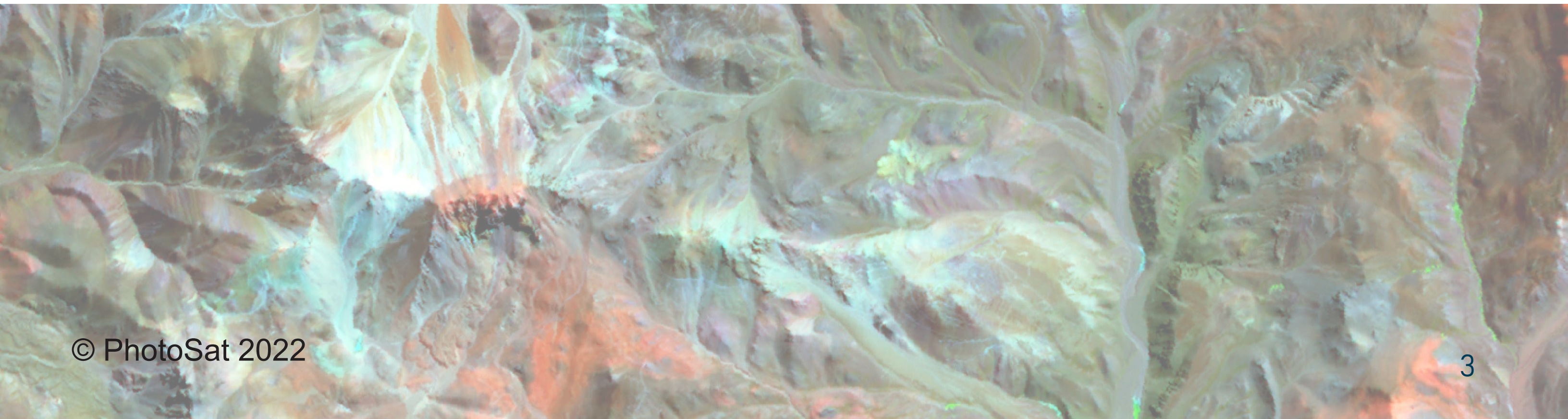

List of Figures

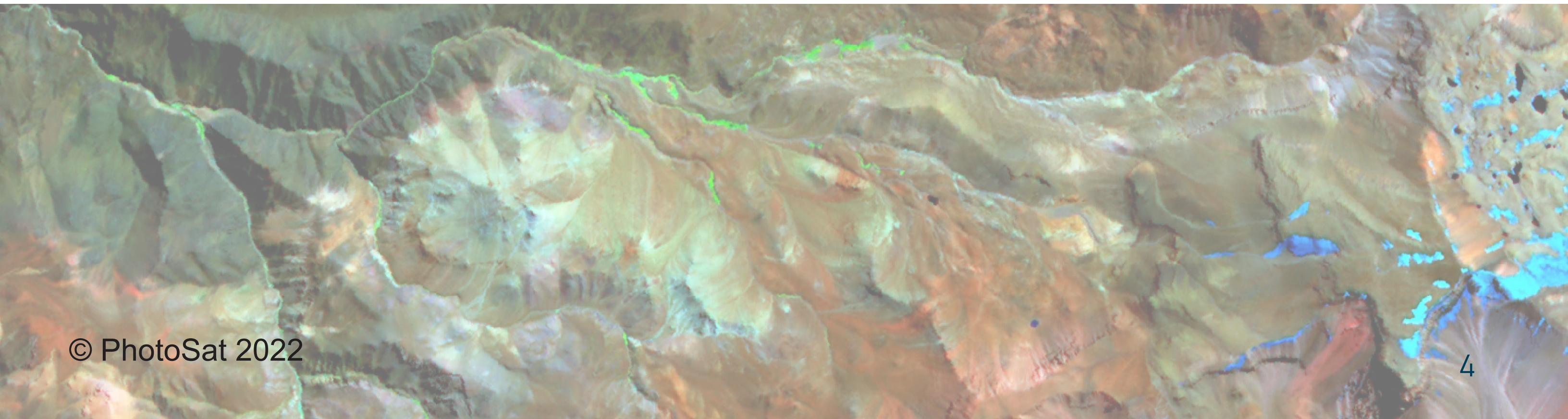

Abstract

The Cerro Casale and Caspiche gold-copper deposits are located in the Maricunga Belt of northern Chile, 110 km southeast of Copiapo.

The Maricunga Belt encompasses numerous large hydrothermal alteration zones hosted by volcanic rocks and high level stocks which intruded them. Mineralization includes gold +/- copper-rich porphyry and precious-metal epithermal styles, formed during late Oligocene and Miocene hydrothermal events. (Sillitoe *et al.* 1991)

Both deposits were discovered in the 1980's and have undergone extensive exploration. Currently, the two deposits form part of the Norte Abierto JV between Newmont Goldcorp and Barrick Gold.

In this alteration report, PhotoSat produces a series of regional alteration mineral maps from ASTER satellite imagery for the area around the two deposits.

For results, read the full alteration report.

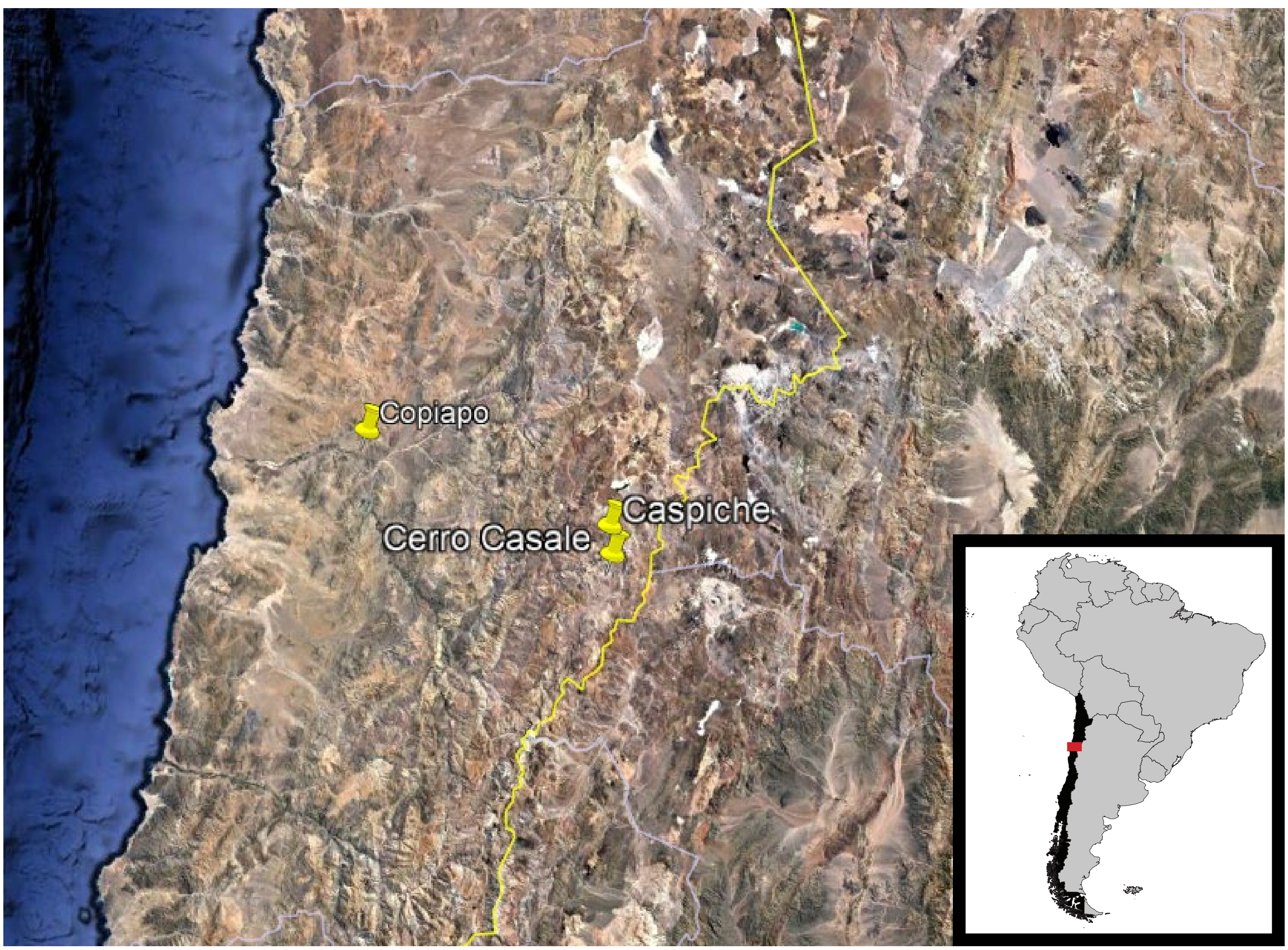

Figure 1: Location of Cerro Casale and Caspiche deposits

Introduction

This report shows the distribution of alteration minerals around the Cerro Casale and Caspiche deposits.

Regional Geology

The Cerro Casale and Caspiche gold-copper deposits form part of the Norte Abierto JV between Newmont Goldcorp and Barrick Gold.

The Cerro Casale and Caspiche deposits are located in the Aldebaran sub-district of the Maricunga Volcanic Belt. The Maricunga Belt is comprised of a series of coalescing composite, Miocene andesitic to rhyolitic volcanic centres that extend for 200 km along the western crest of the Andes.

Reverse faults parallel to the axis of the Andes have caused uplift of hypabyssal intrusive rocks beneath the extrusive volcanics. In turn, this has exposed porphyry-hosted gold and copper deposits in the Aldebaran region.

Cerro Casale Deposit

At Cerro Casale, gold-copper mineralization occurs in quartz-sulphide and quartz-magnetite-specularite veinlet stockworks developed in dioritic to granodioritic intrusives and in adjacent intermediate to felsic volcanic rocks. Mineralization appears to be most closely related to strong potassic to phyllic alteration of the latest phases of intermediate to felsic intrusives and associated intrusive and hydrothermal breccias. (Norto Abierto (Cerro Casale) Project Geology)

Caspiche Deposit

The Caspiche deposit lies 12 km north of the Cerro Casale deposit. At Caspiche, gold-copper mineralization is centered on a composite diorite to quartz diorite porphyry stock intruding felsic volcanic rocks. Within the deposit, five outward-younging phases are routinely distinguished.

The gold-copper mineralization in the lower half of the deposit accompanies quartz ± magnetite-veined, potassic-altered rocks. Shallower mineralization occurs within quartz-kaolinite–dominated, advanced argillic alteration. Upper parts of the advanced argillic zone are characterized by siliceous ledges, some auriferous, composed of vuggy residual quartz and/or silicified rock.

A relatively minor, shallowly inclined zone of intermediate sulfidation epithermal gold-zinc mineralization, comprising narrow veinlets and disseminations, abuts a late-mineral diatreme contact. Post mineral volcanics cover much of the area in the north of the property. Quaternary colluvium overlies most of the property. (Sillitoe et al, 2013)

Methods

Launched in 2019, our current alteration mineral mapping process is an application of spectral analysis to satellite imagery, using proprietary data processing with deep learning technology.

PhotoSat works with either ASTER or WorldView-3 (WV-3) satellite imagery. Since the short-wave infrared (SWIR) ASTER sensor is no longer operational, all ASTER satellite imagery is from the archive.

Spectral Resolution

The ASTER satellite is equipped with multispectral imaging instruments capable of collecting information from 14 sensor bands.

With ASTER, these bands cover specific wavelengths of the visible and near-infrared (VNIR), SWIR, and thermal infrared (TIR) parts of the electromagnetic (EM) spectrum (Fig. 2).

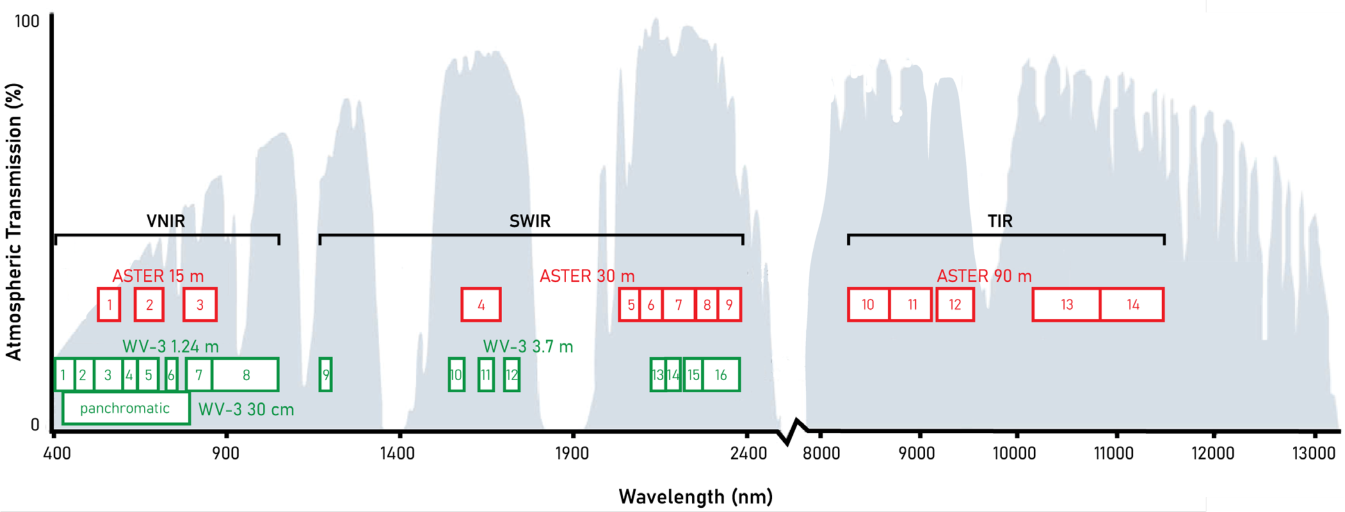

Figure 2: Bands detected by ASTER and WV-3

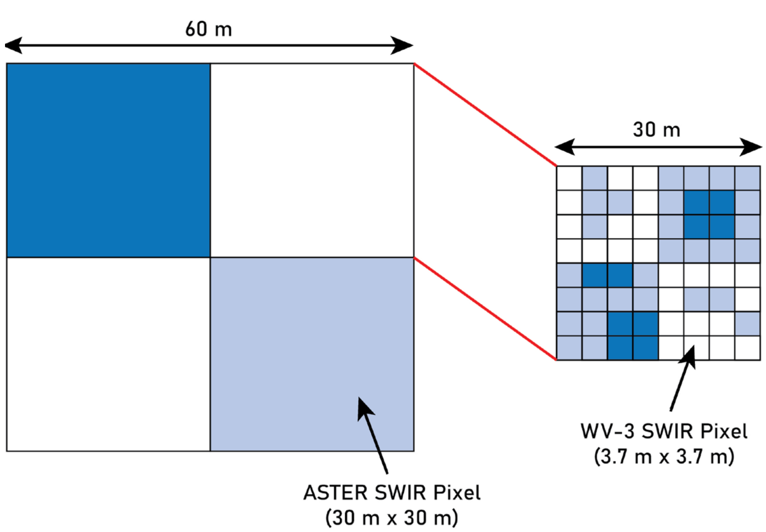

Figure 3: SWIR pixel size of ASTER and WV-3

Spatial Resolution

ASTER imagery has a VNIR pixel size of 15 m, a SWIR pixel size of 30 m, and a TIR pixel size of 90 m.

Because of its large pixel size, ASTER imagery is suitable for alteration mapping at a regional scale.

Spectral Matching

Minerals have unique spectral characteristics that can be used to identify them. To positively identify a mineral, we look for and examine diagnostic features in the spectral profile or "signature".

- **Slope:** Changes in slope between spectral bands can be used to identify some minerals. Not all slopes are distinct from each other, so the slope alone may be insufficient as a means of identification.
- **Absorption features:** Minerals have unique absorption features in their spectral signature, which appear as dips in the profile.

The spectral profile of each pixel in a satellite photo can be matched or compared to reference spectral profiles of known minerals and other surface materials using resources such as the USGS Spectral Library (Fig. 4).

PhotoSat maintains an internal library of reference spectral profiles for this purpose, collected from a variety of sources.

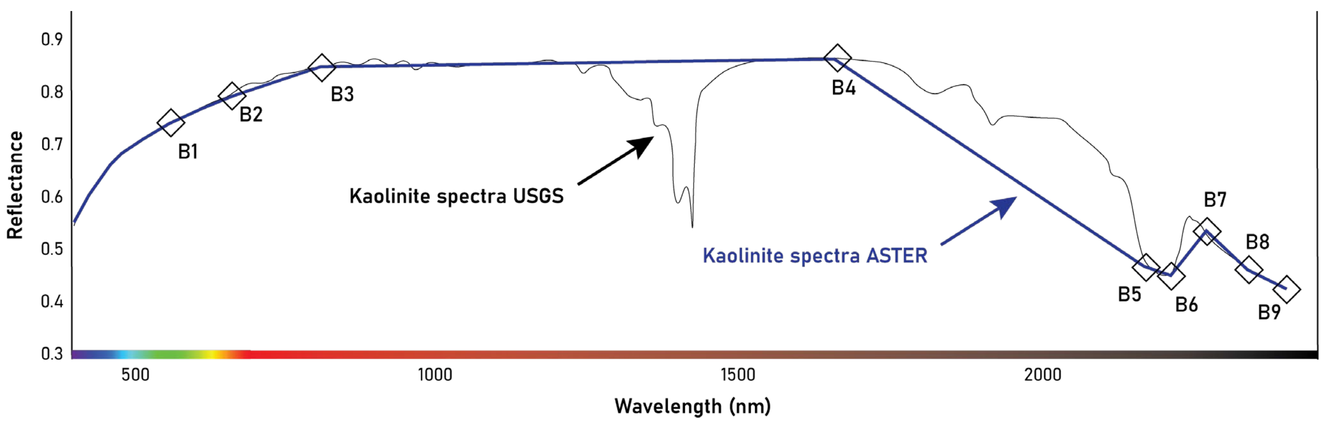

Figure 4a: Spectral profile of kaolinite with ASTER

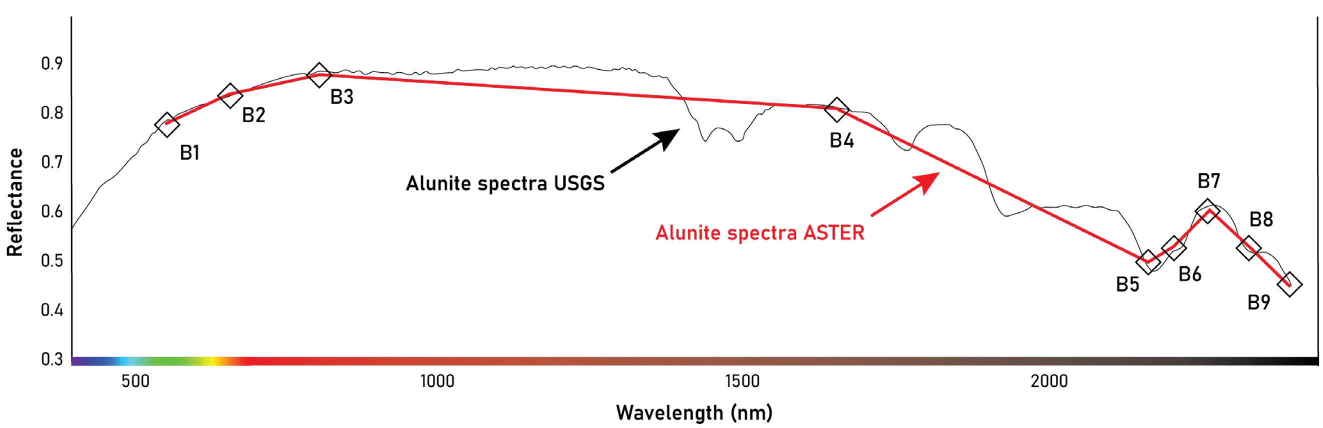

Figure 4b: Spectral profile of alunite with ASTER

Deep Learning

PhotoSat uses deep learning technology in its data processing.

Reliability and Repeatability

PhotoSat's data processing is governed by proprietary algorithms which create repeatable results.

This consistency applies to alteration mapping at property scale, and also between alteration projects that are located in different regions.

CNN Training

In alteration mapping, the use of convolutional neural networks (CNN) allows for continual improvement of the process.

By conducting alteration mapping tests in areas rich in surficial data, we can train the CNN, therefore improving future performance and assessing the reliability of our current alteration mapping processes.

Results

This report includes a separate alteration image for each mineral detected. These are found in Figure 6 to Figure 16.

Geology Enhanced Colour

This geology enhanced image (Fig. 5) shows the area around the Cerro Casale and Caspiche deposits.

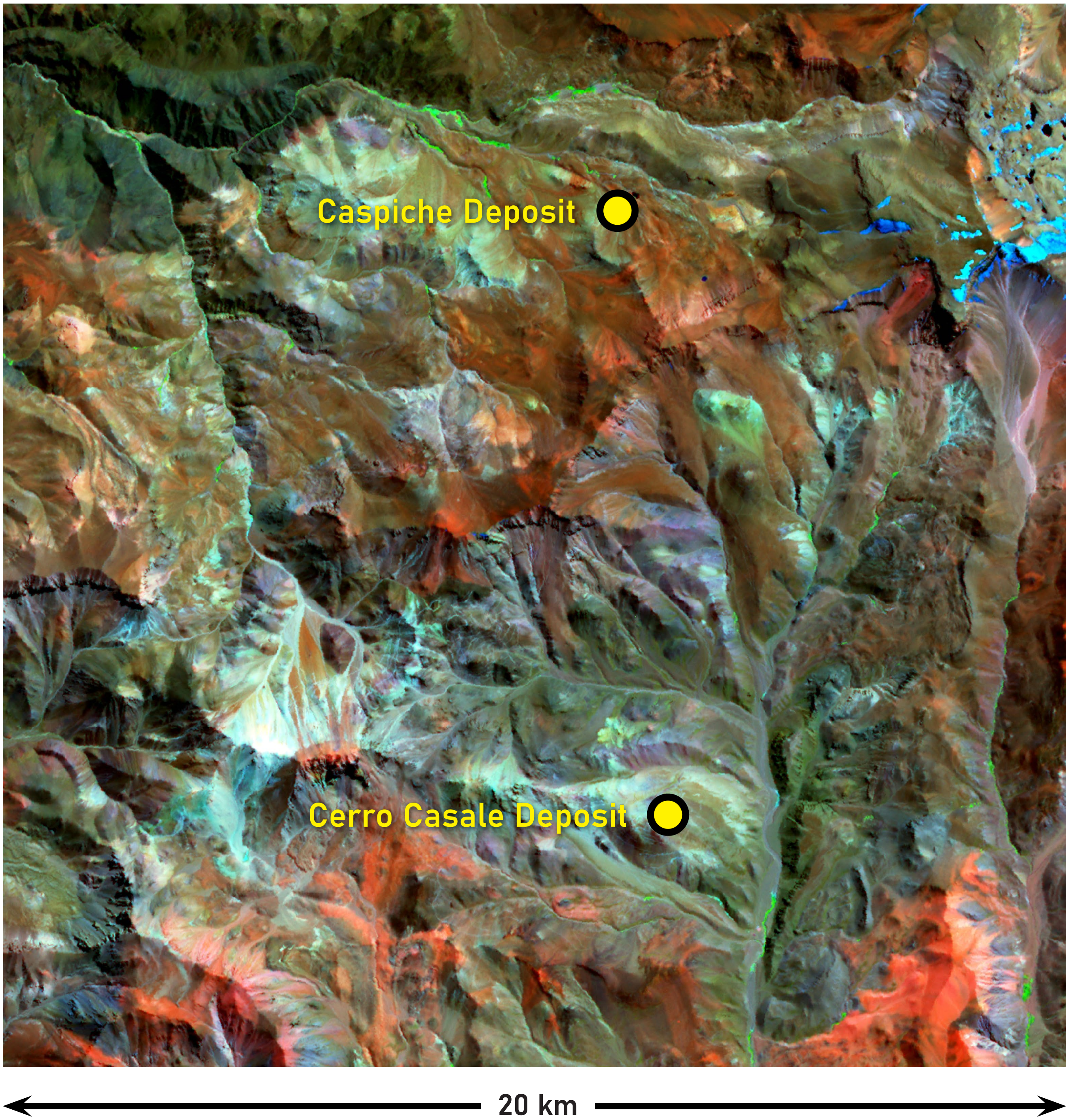

Figure 5: Geology enhanced image of Cerro Casale and Caspiche deposits

Alunite

This alteration mineral map (Fig. 6) for alunite was produced from 14-band ASTER satellite imagery.

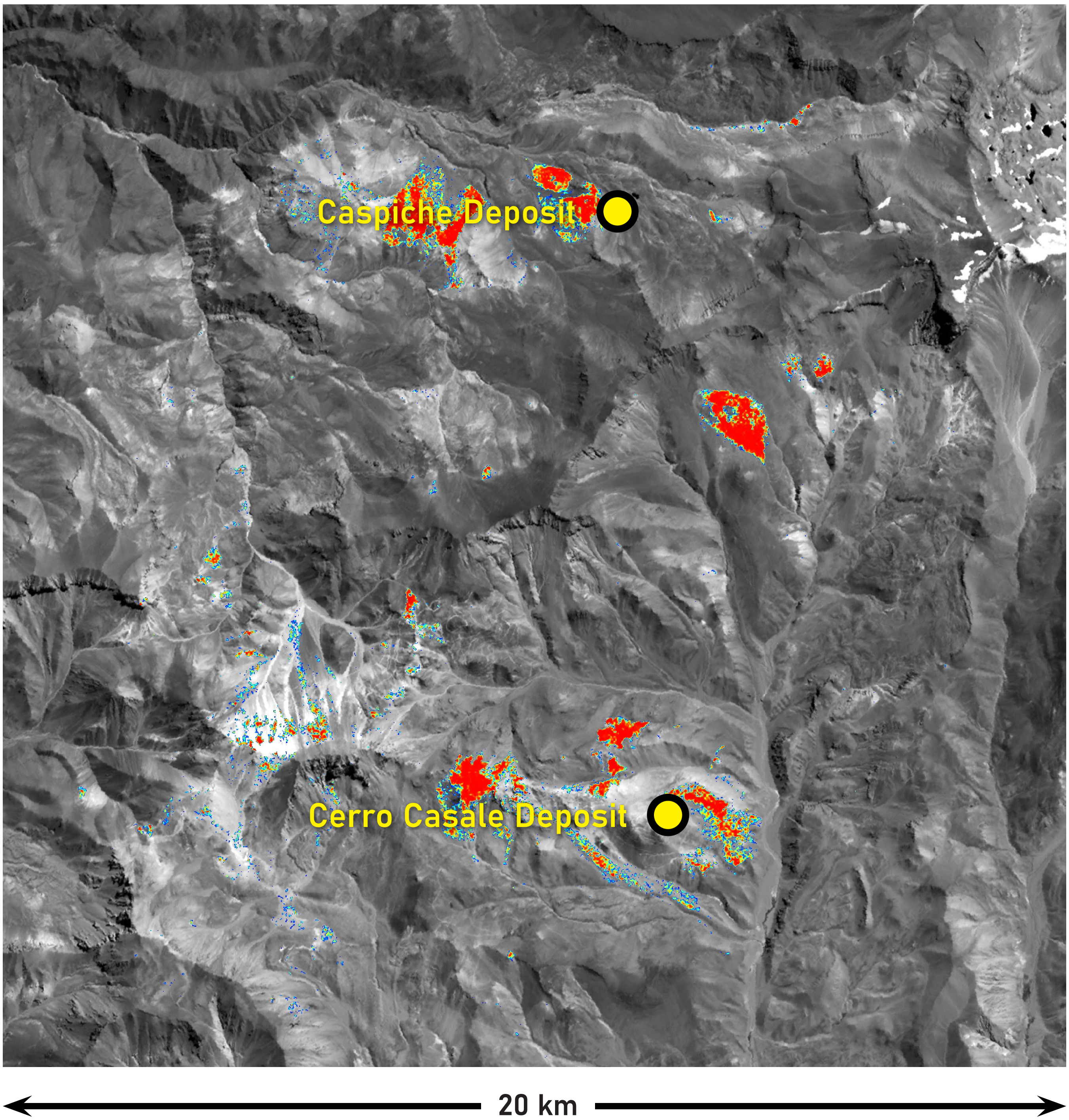

Figure 6: Alteration map of alunite with ASTER imagery

Kaolinite

This alteration mineral map (Fig. 7) for kaolinite was produced from 14-band ASTER satellite imagery.

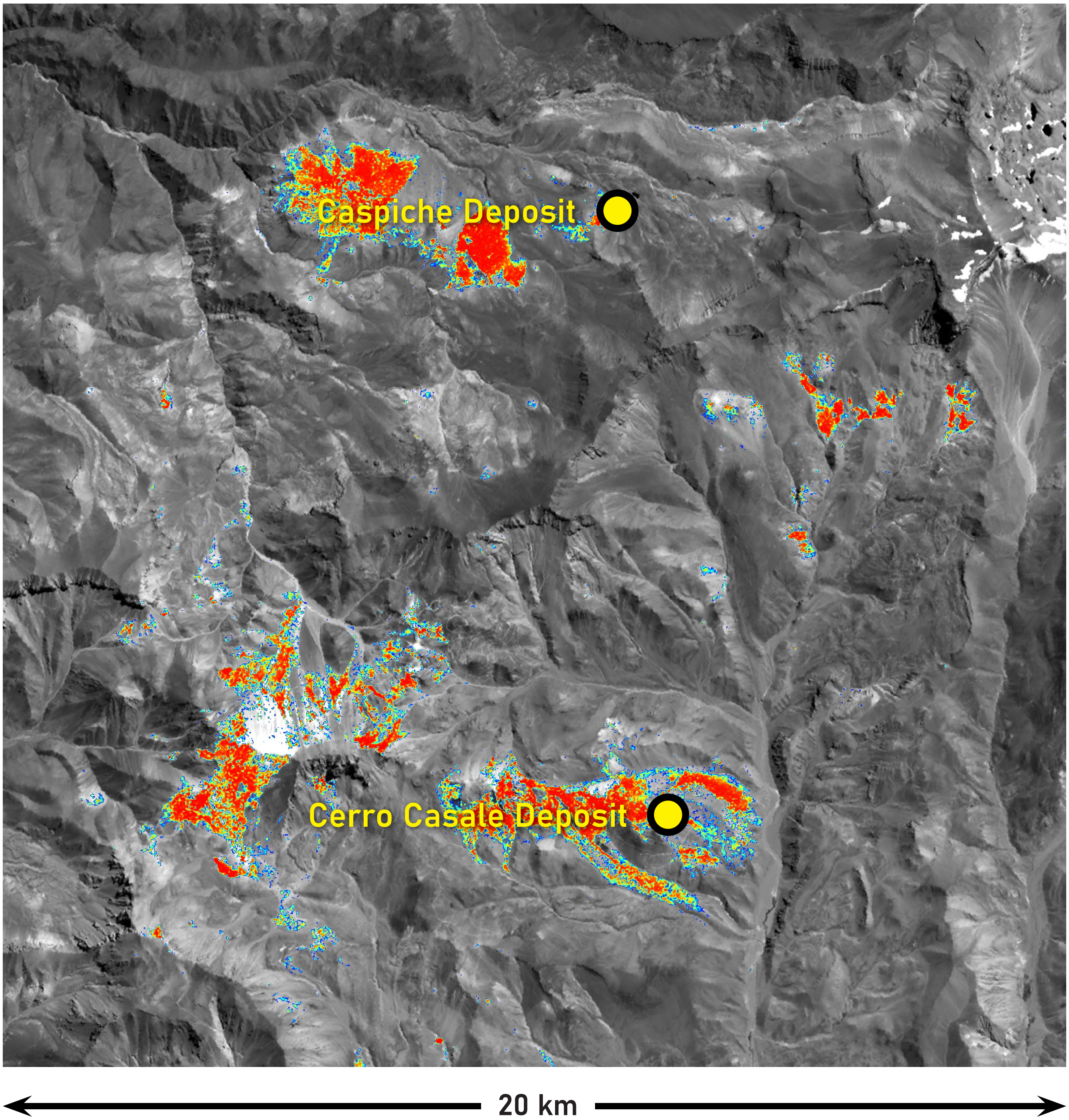

Figure 7: Alteration map of kaolinite with ASTER imagery

Buddingtonite

This alteration mineral map (Fig. 8) for buddingtonite was produced from 14-band ASTER satellite imagery.

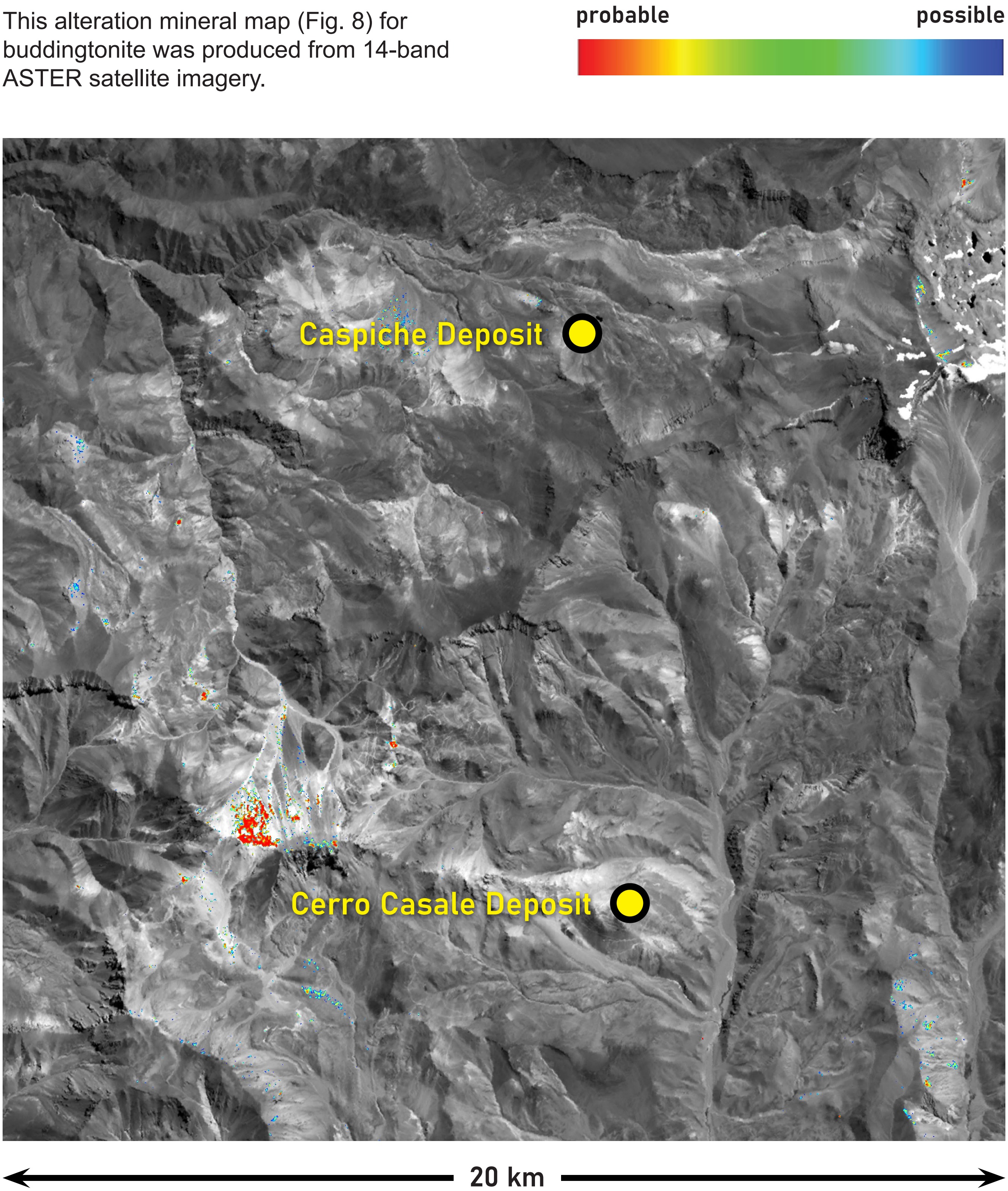

Figure 8: Alteration map of buddingtonite with ASTER imagery

Opal

This alteration mineral map (Fig. 9) for opal was produced from 14-band ASTER satellite imagery.

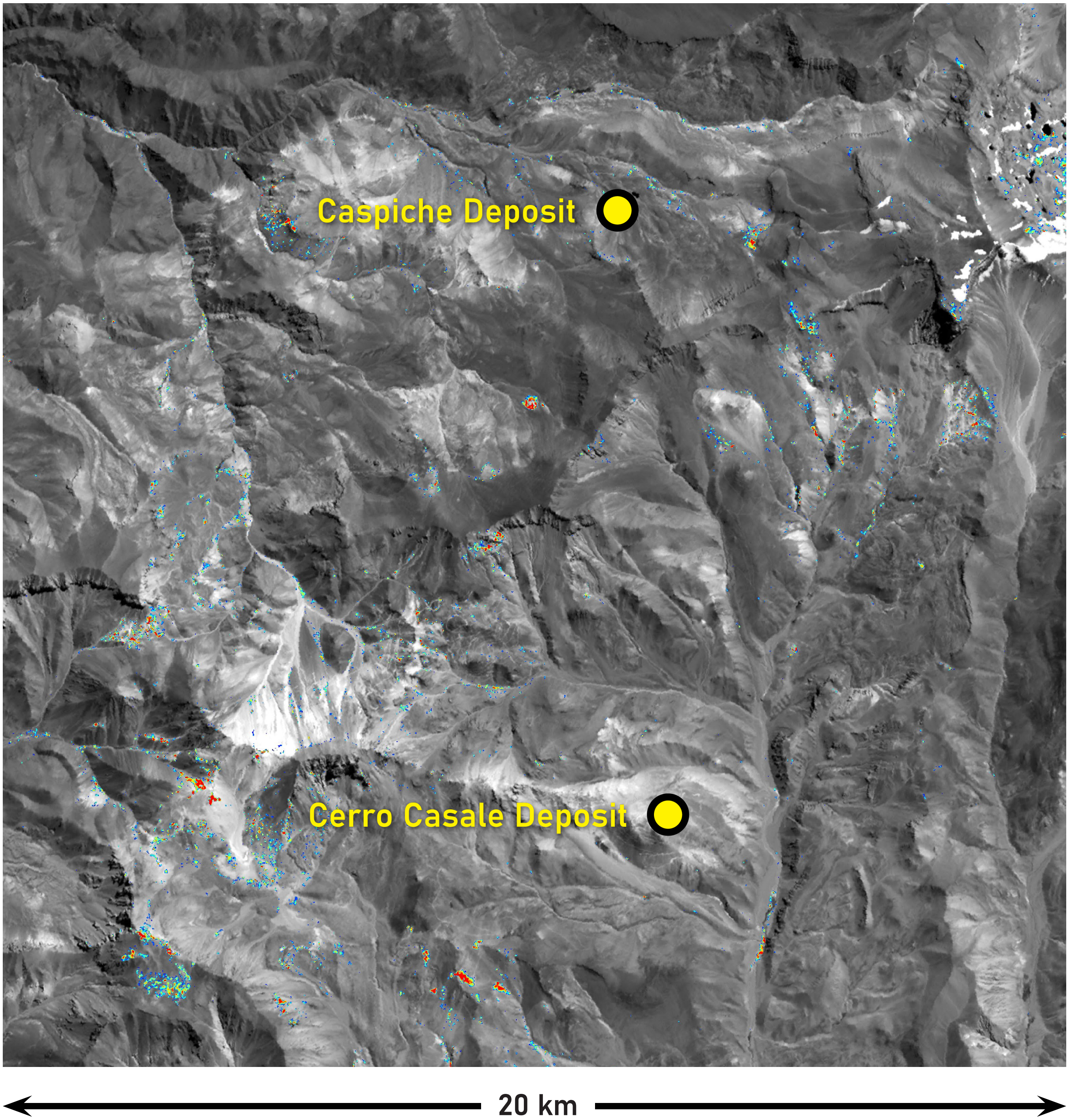

Figure 9: Alteration map of opal with ASTER imagery

Calcite

This alteration mineral map (Fig. 10) for calcite was produced from 14-band ASTER satellite imagery.

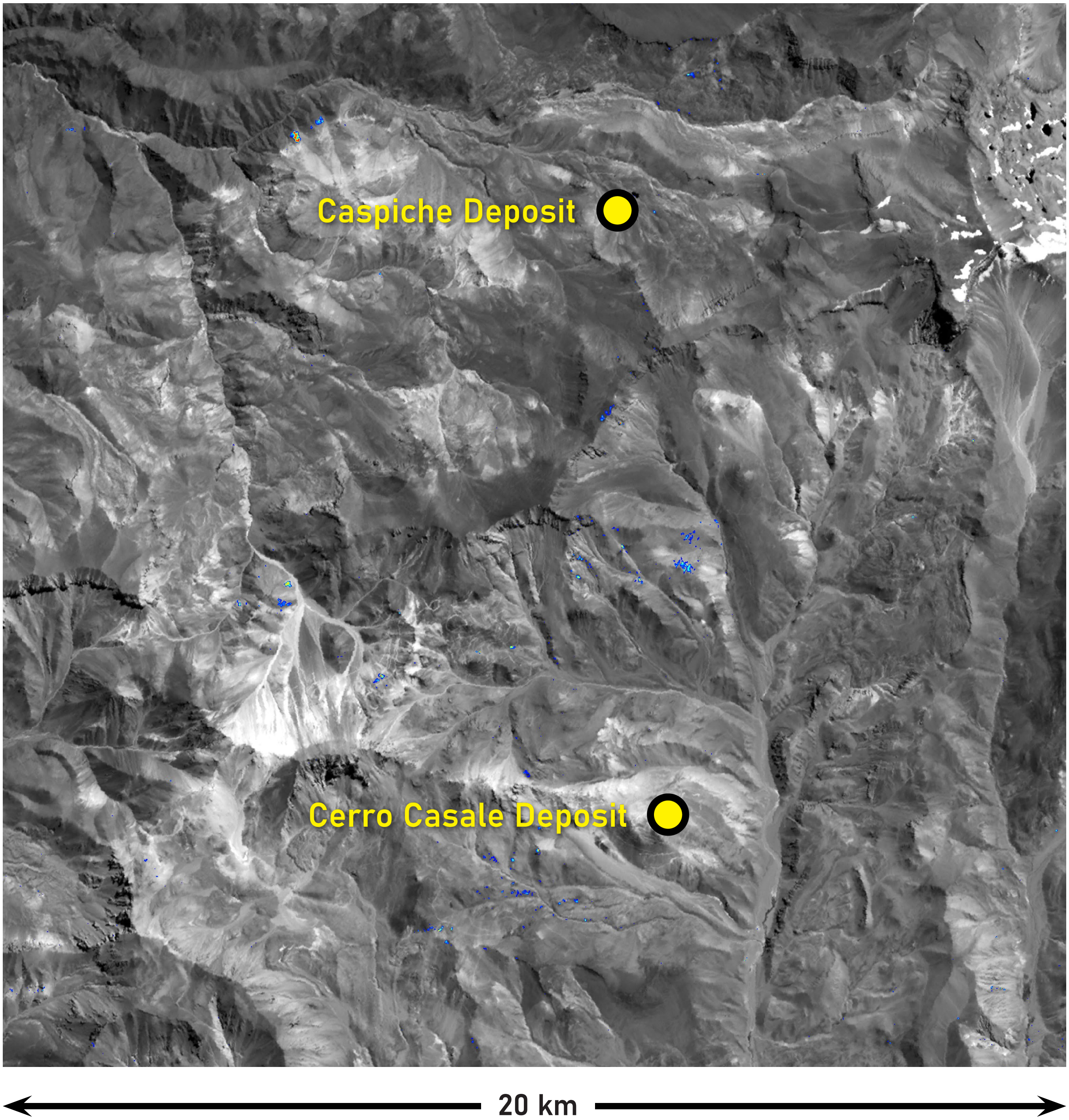

Figure 10: Alteration map of calcite with ASTER imagery

Chlorite

This alteration mineral map (Fig. 11) for chlorite was produced from 14-band ASTER satellite imagery.

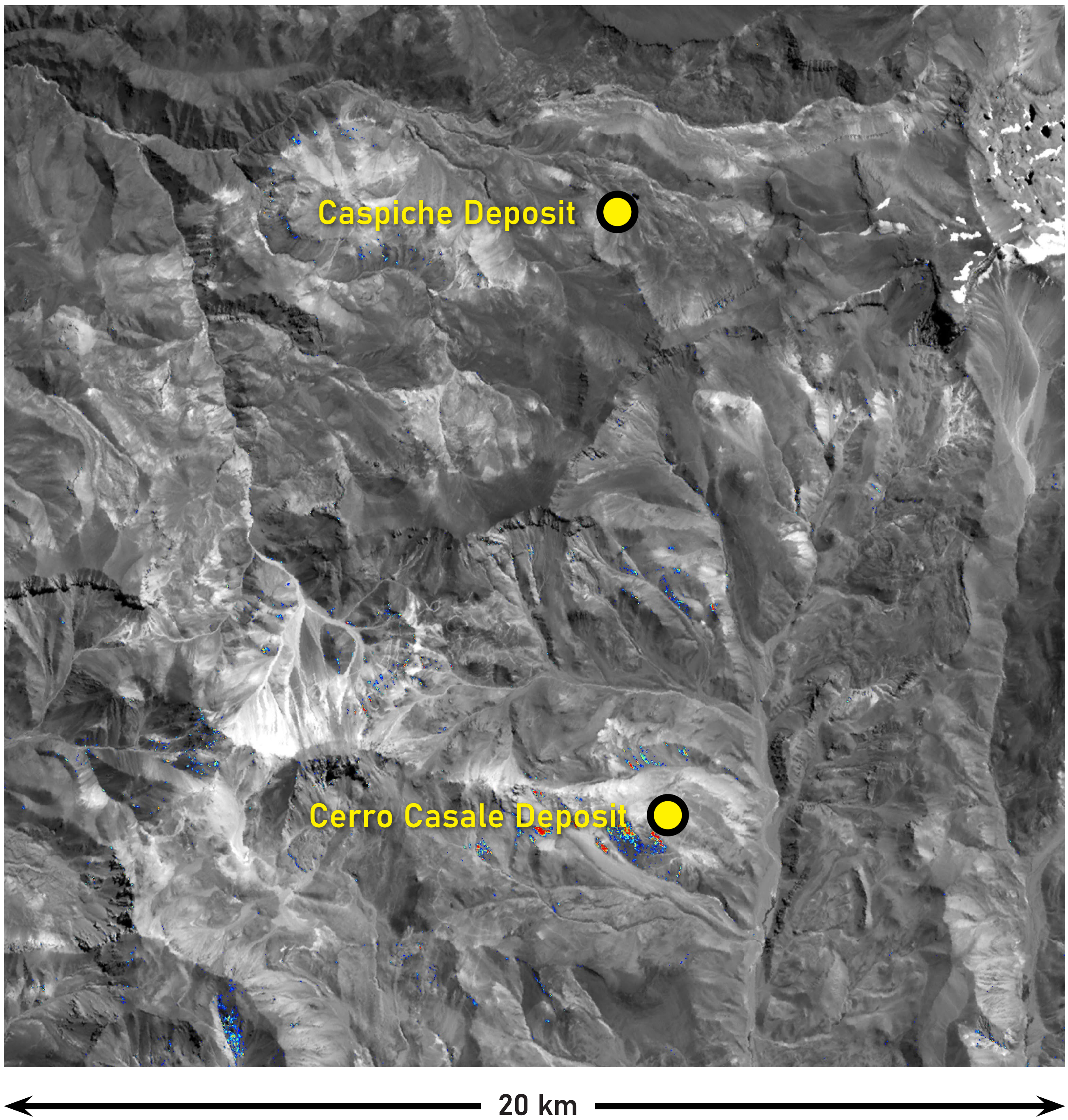

Figure 11: Alteration map of chlorite with ASTER imagery

Sericite

This alteration mineral map (Fig. 12) for sericite was produced from 14-band ASTER satellite imagery.

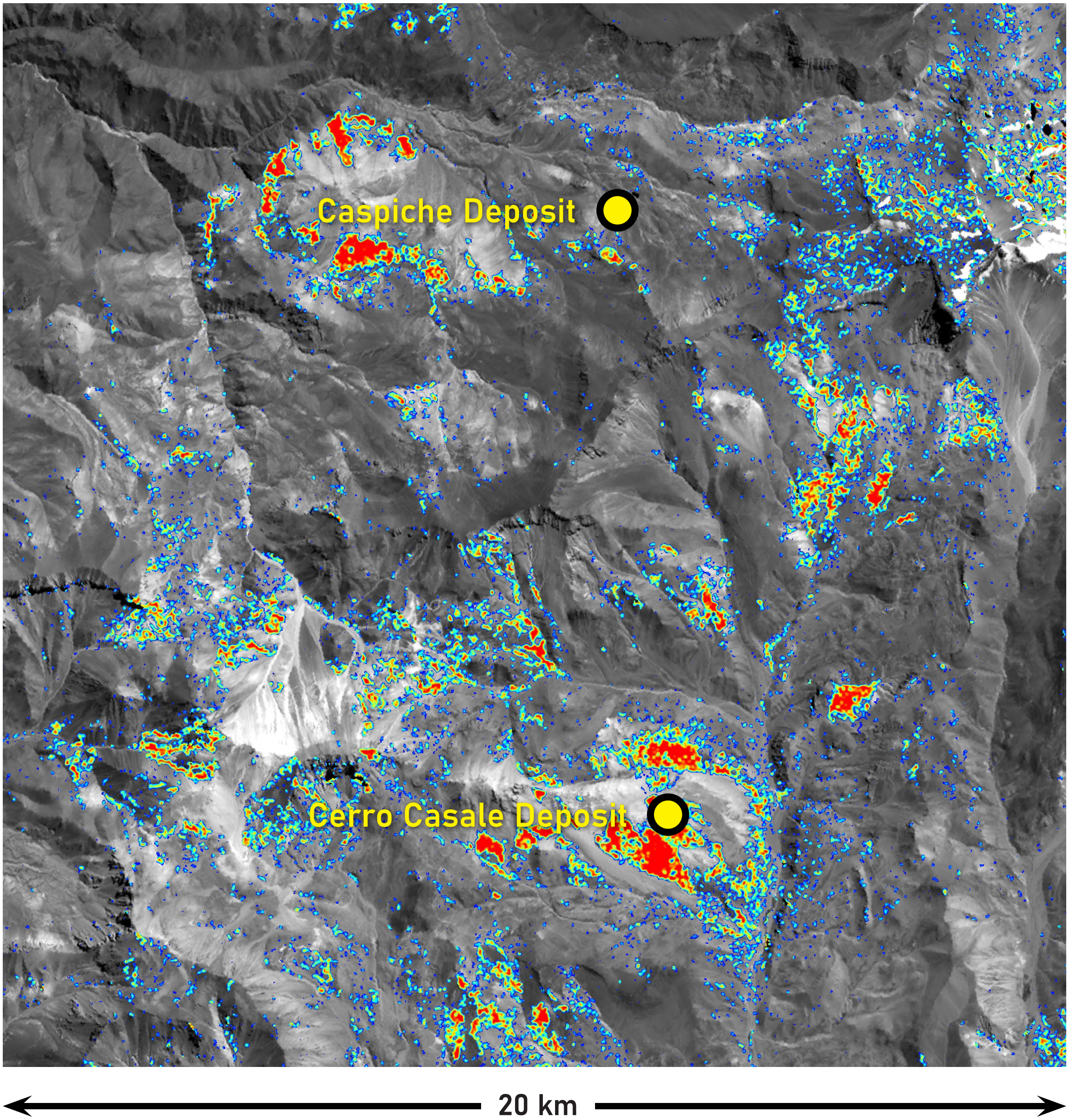

Figure 12: Alteration map of sericite with ASTER imagery

Goethite

This alteration mineral map (Fig. 13) for goethite was produced from 14-band ASTER satellite imagery.

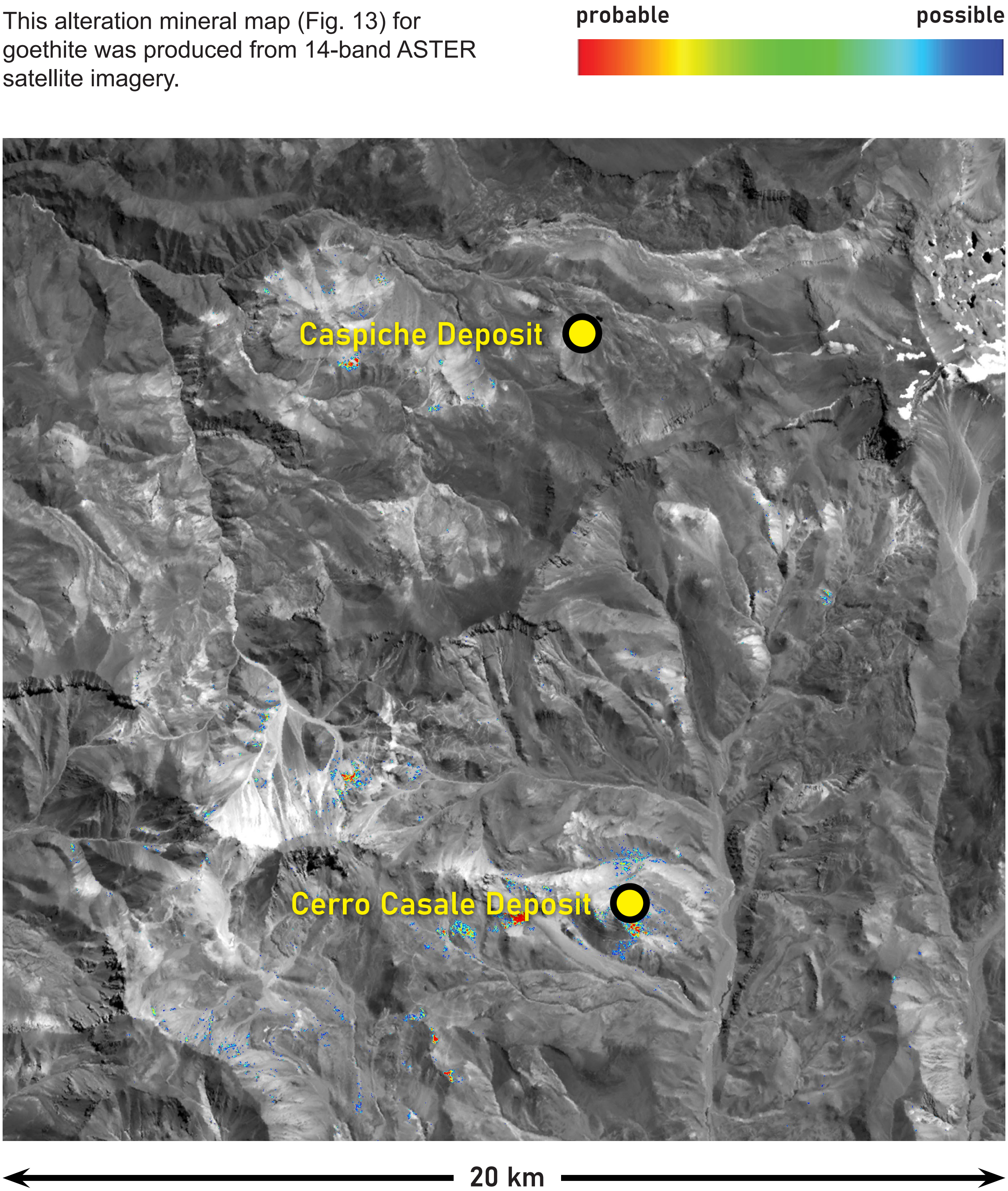

Figure 13: Alteration map of goethite with ASTER imagery

Jarosite

This alteration mineral map (Fig. 14) for jarosite was produced from 14-band ASTER satellite imagery.

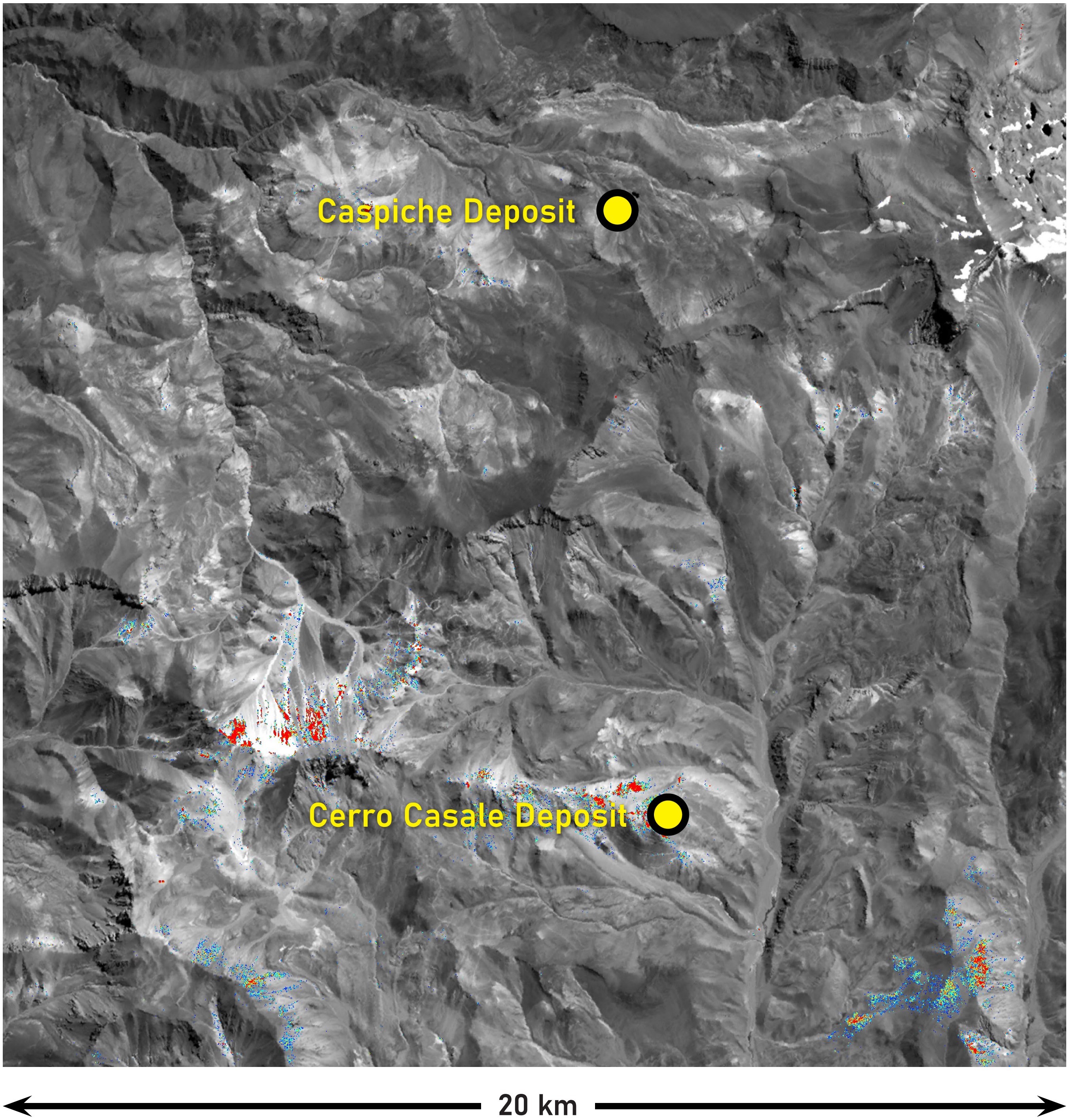

Figure 14: Alteration map of jarosite with ASTER imagery

Hematite

This alteration mineral map (Fig. 15) for hematite was produced from 14-band ASTER satellite imagery.

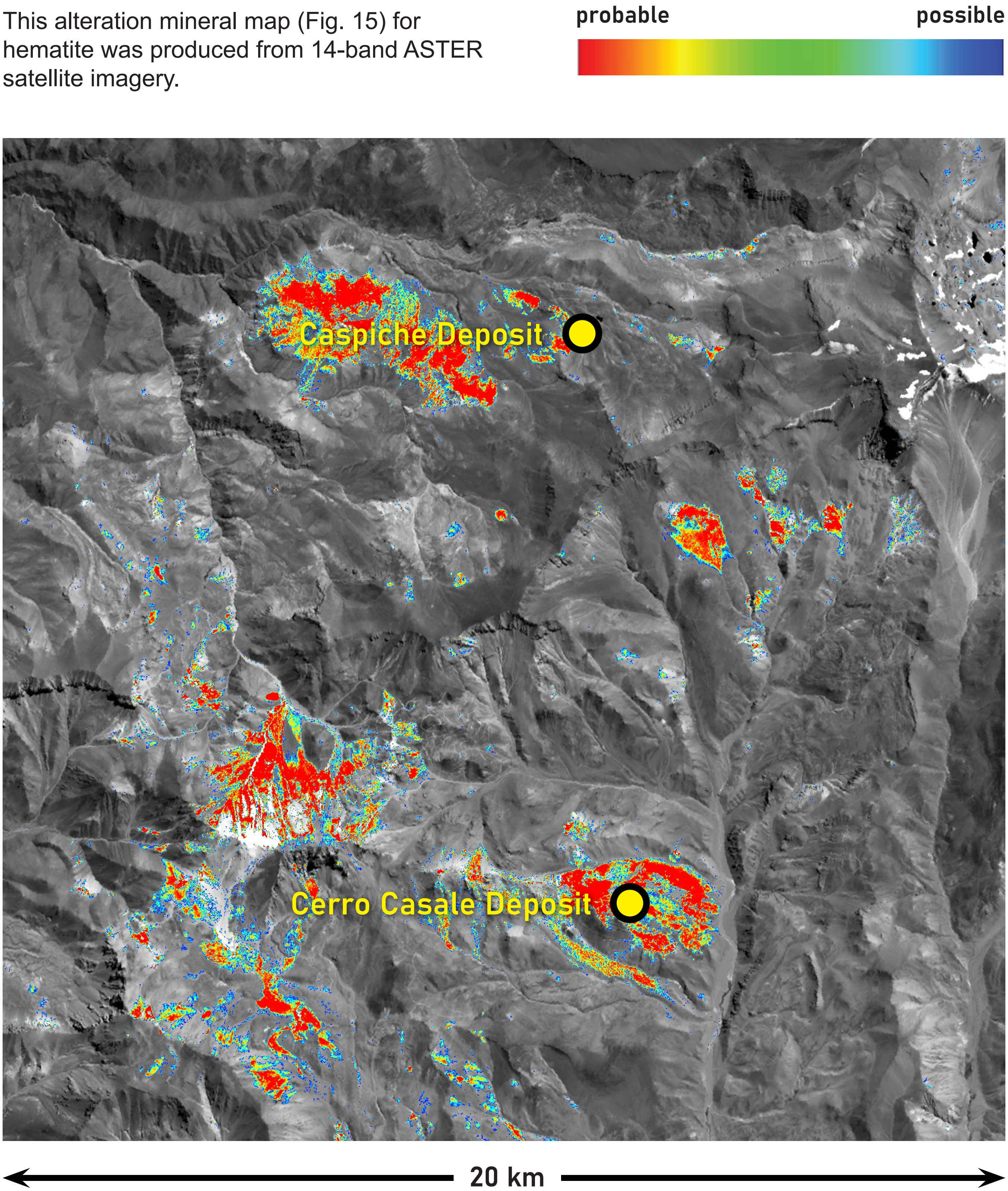

Figure 15: Alteration map of hematite with ASTER imagery

Iron Oxide

This alteration mineral map (Fig. 16) for iron oxide was produced from 14-band ASTER satellite imagery.

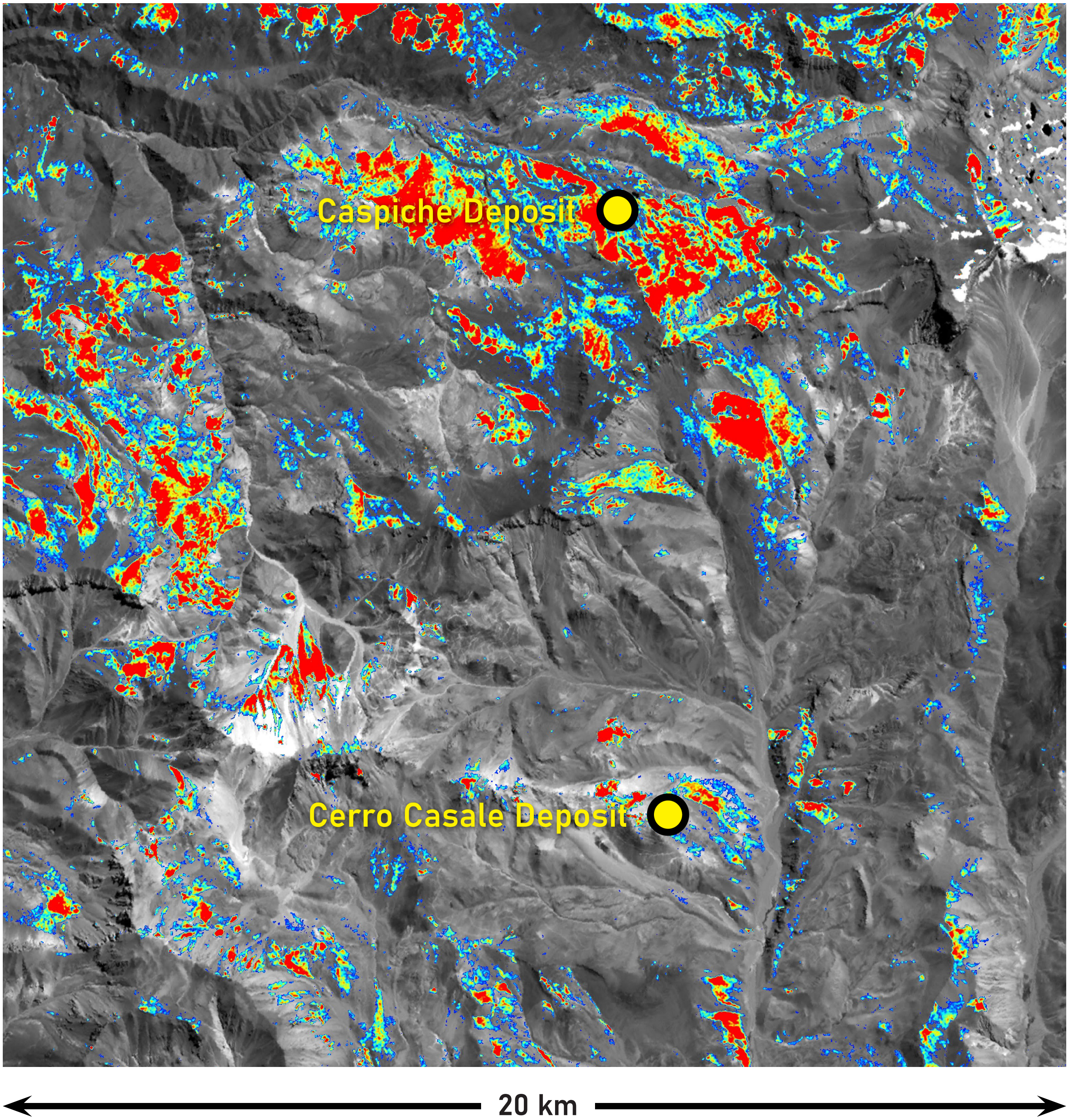

Figure 16: Alteration map of iron oxide gossans with ASTER imagery

Silica

This alteration mineral map (Fig. 17) for silica was produced from 14-band ASTER satellite imagery at a pixel size of 75 m.

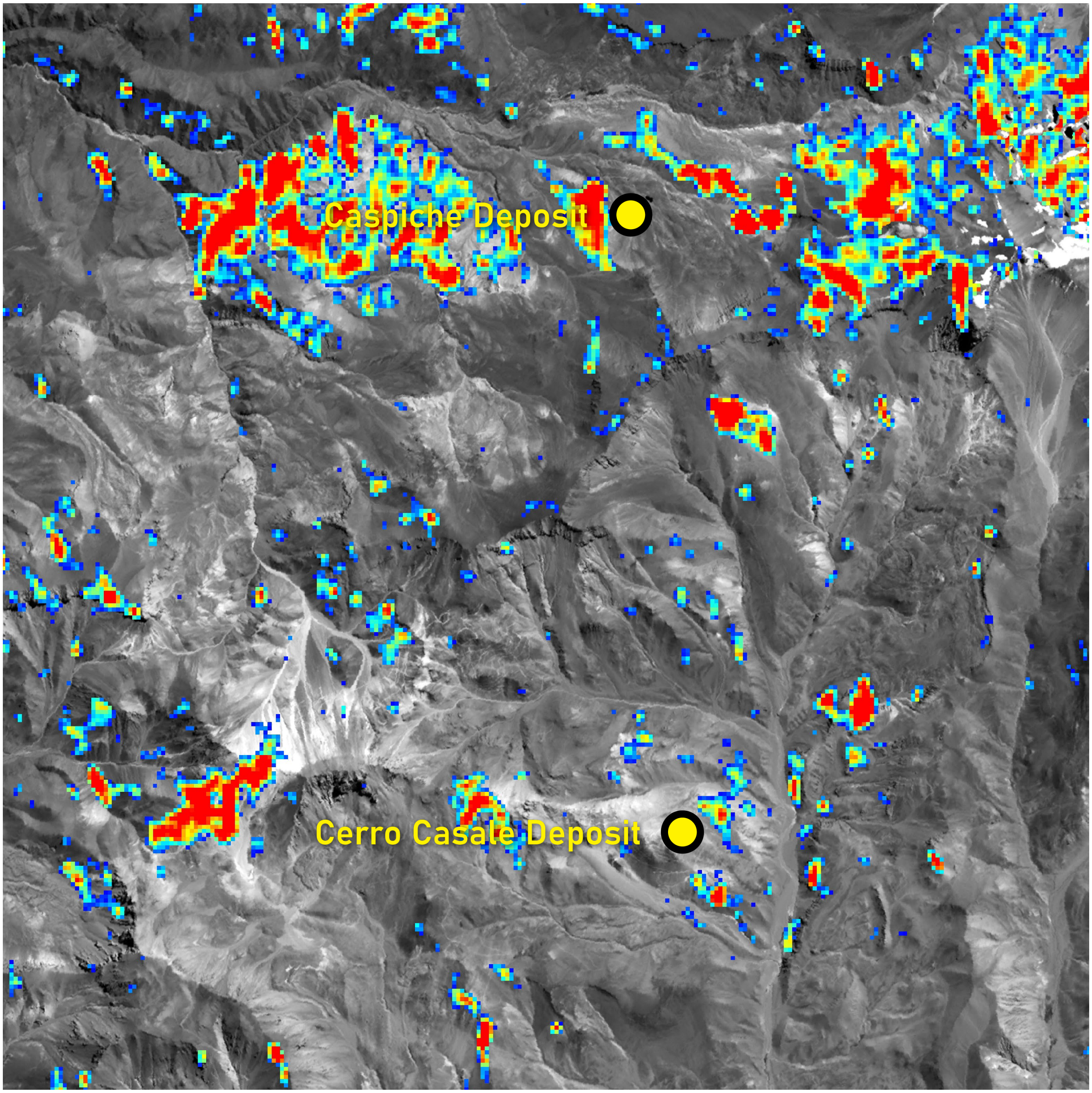

20 km

Figure 17: Alteration map of silica with ASTER imagery

Alteration Compilation

This map (Fig. 18) shows the alteration minerals detected around the Cerro Casale and Caspiche deposits.

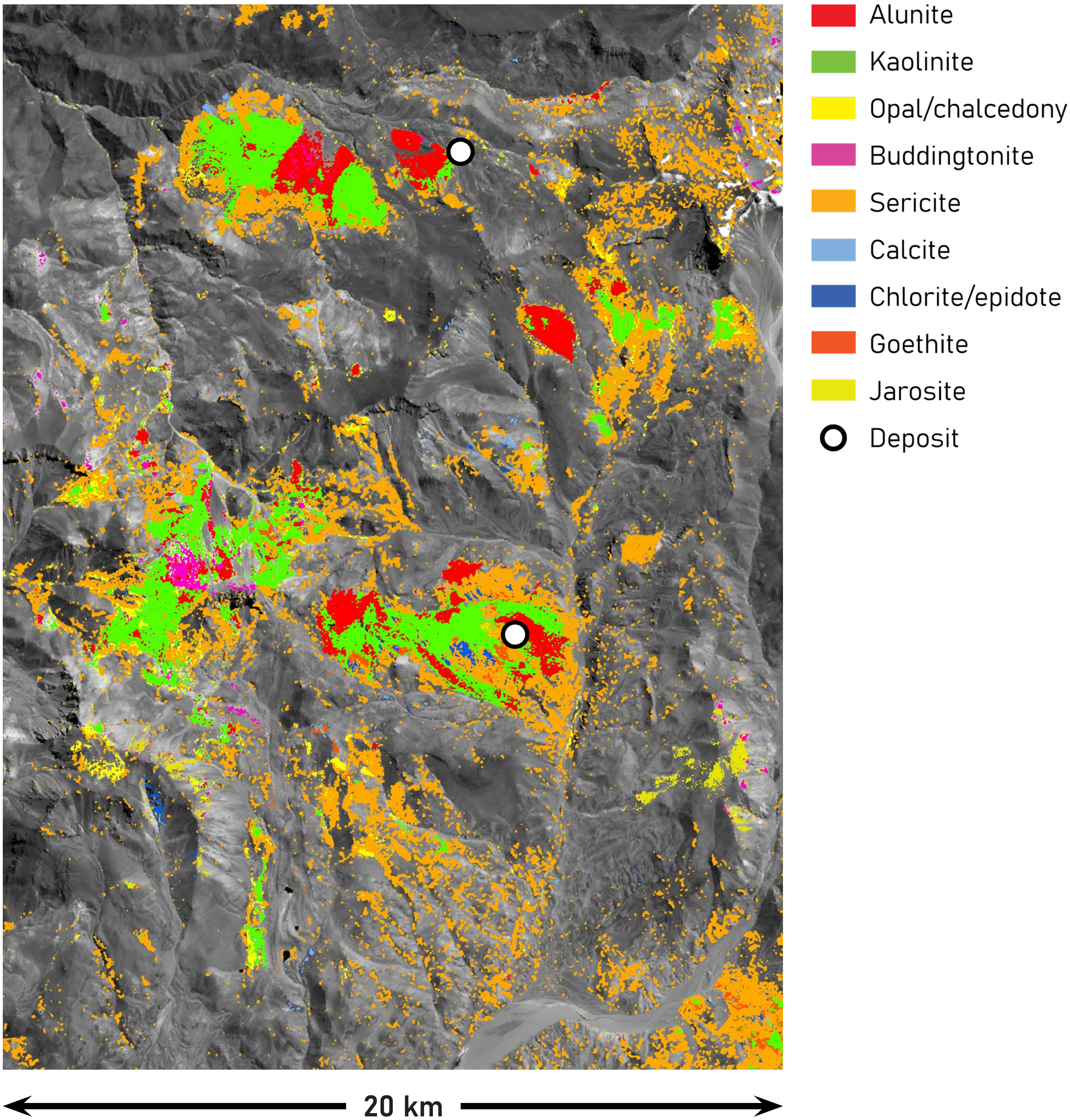

Figure 18: Compilation map of alteration minerals

Discussion

From testing, we know that certain alteration minerals can be reliably mapped through PhotoSat's data processing with deep learning technology.

If alteration is present at surface and visible in satellite photos, PhotoSat's alteration mineral mapping produced from ASTER satellite imagery can detect the following minerals:

Micas

The result for sericite, or white mica, may consist of one or some combination of:

- **Muscovite:** $KAl_2(Si_3Al)O_{10}(OH,F)_2$
- **Paragonite:** $NaAl_2[(OH)_2|AlSi_3O_{10}]$
- **Illite:** $(K,H_3O)(Al,Mg,Fe)_2(Si,Al)_4O_{10}[(OH)_2,H_2O]$

Iron Minerals

PhotoSat can identify:

- **Iron Oxide Gossans:** many different red, orange, and brown iron oxide minerals.
- **Hematite:** $Fe^{3+}{}_2O_3$
- **Goethite:** $Fe^{3+}O(OH)$
- **Jarosite:** $KFe^{3+}{}_3(SO_4)_2(OH)_6$

Clay Minerals

PhotoSat can identify:

- **Alunite:** $(Na,K)Al_3(SO_4)_2(OH)_6$
- **Kaolinite:** $Al_2Si_2O_5(OH)_4$

Other Minerals

PhotoSat can identify:

- **Silica:** SiO_2
- **Opal/Chalcedony*:** $SiO_2 \cdot nH_2O$
- **Buddingtonite:** $NH_4AlSi_3O_8$
- **Calcite:** $CaCO_3$
- **Chlorite/Epidote****
  $(Mg,Fe,Li)_6AlSi_3O_{10}(OH)_8$ / $Ca_2(Al,Fe)_2(SiO_4)(OH)_2$

Context Images

PhotoSat also includes the following images with its ASTER alteration mapping package:

- 12.5 m Geology enhanced colour image
- 12.5 m Vegetation intensity
- 12.5 m Greyscale image

*PhotoSat cannot differentiate between opal and chalcedony with 16-band WorldView-3.

**PhotoSat cannot differentiate between chlorite and epidote with 16-band WorldView-3.